

**PREPARATION AND CHARACTERIZATION OF
MUSCOVITE-CARBON NANOTUBES/EPOXY LAYERED
SILICATE NANOCOMPOSITES**

by

NUR SURAYA ANIS BINTI AHMAD BAKHTIAR

**Thesis submitted in fulfillment of the
requirements for the degree of
Doctor of Philosophy**

September 2019

ACKNOWLEDGEMENT

Alhamdulillah, all praises to Allah S.W.T. for His kindness and blessing, whom gave me strength and healthy to finish up my research entitled *PREPARATION AND CHARACTERIZATION OF MUSCOVITE-CARBON NANOTUBES/EPOXY LAYERED SILICATE NANOCOMPOSITES* with efficiently, proper and enjoyable.

First of all, I would like to express my sincere gratitude to my supervisor, Professor Dr Hazizan Md Akil for his kindness, encouragement, valuable information, suggestion and guidance.

Deepest thanks and appreciation to my parents, Ahmad Bakhtiar bin Mahayuddin and my late mother Salmah bt Haji Kassim, my husband, Raja Mohamad Faiz bin Raja Othman and also not forgotten, my beloved daughters, Raja Aisyah Humaira and Raja Fatimah Azzahra for their prayers, encouragement and most valuable moral support to complete the research during all the time.

Great deals appreciate go to contribution of my school- School of Materials and Minerals Engineering, Universiti Sains Malaysia and all the staff that helping me to complete this project.

I am grateful to my colleagues and friends, who's always give me advices and encouragement during good or bad conditions.

Last but not least, I feel gratitude to Research University Grant (1001/PBAHAN/814137) of University Science Malaysia and MyBrain15 for the financial assistance.

TABLE OF CONTENTS

	Page
ACKNOWLEDGEMENT	ii
TABLE OF CONTENTS	iii
LIST OF TABLES	viii
LIST OF FIGURES	iv
LIST OF ABBREVIATIONS	xiv
LIST OF SYMBOLS	xvi
ABSTRAK	xv
ABSTRACT	xvii
 CHAPTER ONE: INTRODUCTION	
1.1 Background	1
1.2 Problem Statement	3
1.3 Objectives of the Research	7
1.4 Structure of the Thesis	7
 CHAPTER TWO: LITERATURE REVIEW	
2.1 Polymer Nanocomposites	9
2.2 Layered Silicate	11
2.2.1 Montmorillonite	13
2.2.2 Muscovite	14
2.3 Muscovite Clay Modification	15
2.3.1 Grinding and Delamination	16
2.3.2 Ion Exchange Reaction	17
2.4 Structure and Properties of Modified Layered Silicate	21

2.5	Carbon Nanotubes	22
2.6	Synthesis of Carbon Nanotubes	24
2.6.1	Arc Discharge	24
2.6.2	Laser Ablation	25
2.6.3	Chemical Vapor Deposition	26
2.7	Factors that Affected CNT Growth	26
2.7.1	Catalyst	26
2.7.2	Catalyst Supports	27
2.7.3	Catalyst-Support Interaction	28
2.7.4	Carbon Precursor	29
2.8	Growth mechanism of MWCNT	29
2.9	Carbon Nanotubes Polymer Nanocomposites	31
2.10	Dispersion of Carbon Nanotubes	31
2.10.1	Mechanical Dispersion	32
2.10.2	Chemical Functionalization of Carbon Nanotubes	33
2.10.3	Hybridization of CNTs-Inorganic	34
2.11	Clay-Carbon Nanotubes Hybrid	34
2.12	Preparation of Polymer Nanocomposites	36
2.12.1	In Situ Polymerization	37
2.12.2	Solution Blending	38
2.12.3	Melt Mixing	39
2.13	Epoxy	40
2.14	Epoxy Nanocomposites	41

CHAPTER THREE: EXPERIMENTAL

3.1	Materials	44
3.1.1	Epoxy Resin	44
3.1.2	Hardener	45
3.1.3	Muscovite	45
3.1.4	Lithium Nitrate (LiNO ₃)	46
3.1.5	Cetyltrimethylammonium Bromide (CTAB)	47
3.1.6	Nickel (II) Nitrate Hexahydrate	48
3.1.7	Sodium Hydroxide	48
3.1.8	Multiwalled Carbon Nanotubes (MWCNT)	49
3.2	Gases	50
3.2.1	Methane	50
3.2.2	Nitrogen	50
3.2.3	Hydrogen	51
3.3	Clay Modification	52
3.3.1	LiNO ₃ Treatment of Muscovite	52
3.3.2	Intercalation of Li-muscovite with CTA ⁺	52
3.4	Synthesis of Multiwalled Carbon Nanotubes by Chemical Vapor Deposition (CVD)	53
3.4.1	Catalyst Preparation	53
3.4.2	Synthesis of Mus MWCNT Hybrid	54
3.4.3	Preparation of Mus MWCNT by Physical Mixing	55
3.5	Fabrication of Polymer Nanocomposites	56
3.6	Sample Characterization	58
3.6.1	X-ray Diffraction Analysis (XRD)	58
3.6.2	X-ray Fluorescence (XRF)	59

3.6.3	Energy Dispersive X-Ray (EDX)	59
3.6.4	Inductively Couple Plasma- Optical Emission Spectrometer (ICP)	59
3.6.5	CHN Elemental Analysis	60
3.6.6	Fourier Transmission Infrared (FTIR)	60
3.6.7	Raman Spectroscopy	61
3.7	Mechanical Testing	61
3.7.1	Tensile Test	61
3.7.2	Microhardness Test	61
3.8	Morphological Studies	62
3.8.1	Field Emission Scanning Electron Microscopy (FESEM)	62
3.8.2	High Resolution Transmission Electron Microscopy (HRTEM)	63
3.9	Thermal Testing	
3.9.1	Thermal Conductivity Analysis	63
 CHAPTER FOUR: RESULT AND DISCUSSION		
4.1	Effect of Ion Exchange Treatment on Muscovite Clay	65
4.1.1	X-ray Diffraction (XRD)	65
4.1.2	Elemental Analysis	72
4.1.3	Fourier Transform Analysis (FTIR)	74
4.1.4	Field Emission Scanning Eletron Microscopy (FESEM)	76
4.1.5	High Resolution Transmission Electron Microscopy (HRTEM)	79
4.2	Effect of Organo Muscovite on Synthesis Multiwalled Carbon Nanotubes	84
4.2.1	Field Emission Scanning Electron Microscopy (FESEM)	84

4.2.2	High Resolution Transmission Electron Microscopy (HRTEM)	92
4.2.3	X-Ray Diffraction (XRD)	97
4.2.4	Raman Analysis	100
4.2.5	Fourier Transform Infrared (FTIR)	103
4.3	Mechanical Properties of E/Mus MWCNT Nanocomposites	104
4.3.1	Tensile Properties	104
4.3.2	Microhardness properties	112
4.3.3	X-Ray Diffraction (XRD) analysis	116
4.3.4	Fourier Transform Infrared (FTIR) analysis	119
4.3.5	Field Emission Scanning Electron Microscopy	122
4.3.6	High Resolution Transmission Electron Microscopy	131
4.4	Thermal Properties	141
4.4.1	Thermal Conductivity	141
 CHAPTER FIVE: CONCLUSION AND SUGGESTION FOR FUTURE WORKS		
5.1	Conclusion	147
5.2	Suggestion for Future Work	148
 REFERENCES		149

LIST OF TABLES

		Page
Table 3.1	Properties of purchased epoxy resin (Euro Chemo-Pharma MSDS)	44
Table 3.2	Properties of purchased epoxy hardener (Euro Chemo-Pharma MSDS)	45
Table 3.3	Properties of muscovite (Bidor Mineral Sdn. Bhd. MSDS)	46
Table 3.4	Properties of lithium nitrate supplied (Alfa Aesar MSDS)	47
Table 3.5	Properties of supplied CTAB (Merck MSDS)	48
Table 3.6	Chemical and physical properties of nickel (II) nitrate hexahydrate (MerckChemical MSDS)	48
Table 3.7	Details on Sodium Hydroxide (NaOH)	49
Table 3.8	Properties of MWCNT purchased from SkySpring Nanomaterials Inc.	49
Table 3.9	Information of the purchased methane gas.	50
Table 3.10	Information of the purchased nitrogen gas.	51
Table 3.11	Information of the purchased hydrogen gas.	51
Table 3.12	Description of the filler	56
Table 3.13	Description of the composite samples	57
Table 4.1	Main elemental composition of original Mus, Li-Mus, and CTAB/Li-Mus	74
Table 4.2	Raman Intensity of pure MWCNT, Mus MWCNT PM, Mus MWCNT HYB and O-Mus MWCNT HYB	103
Table 4.3	Summarized of tensile properties for different epoxy nanocomposites systems	112
Table 4.4	Average Vickers Hardness of neat epoxy, E/Mus, E/O-Mus, E/Mus MWCNT PM, E/Mus MWCNT HYB, and E/O-Mus MWCNT HYB with different filler loading	155
Table 4.5	Average data of thermal conductivity at different filler loading	144

LIST OF FIGURES

	Page
Figure 2.1 Classification of polymer layered silicate structure (Loganathan, 2017)	11
Figure 2.2 Structures of 2:1 layered silicate (Alexandre and Dubois, 2000)	12
Figure 2.3 Profile model of Na-montmorillonite (Na-MMT) (Paul and Robeson, 2008; Newton et al., 2017)	13
Figure 2.4 Muscovite structure model (de Poel et al., 2014)	15
Figure 2.5 SEM images of muscovite particles after (a) knife mills, (b) ball mill, (c) vibratory mill and (d) sonication process (Santos et al., 2011)	17
Figure 2.6 Intercalation of layered silicate clays into organo clays via ion exchange intercalation (Anastasiadis et al., 2008)	18
Figure 2.7 Molecular model of the intercalation of Cu into muscovite (Friedrich et al., 2007)	19
Figure 2.8 SEM images of (a) original muscovite and (b) muscovite after LiNO ₃ treatment (Yu et al., 2006a)	20
Figure 2.9 (a) SEM images of OTAC intercalated with Li-muscovite and (b) XRD analysis of the intercalated muscovite (Jia et al., 2015)	21
Figure 2.10 Possible arrangements of alkylammonium (Lagaly, 1986)	22
Figure 2.11 Classification of chirality types (Steel, 2015)	23
Figure 2.12 Schematic representation of rolling graphene layer to create CNT (Wu et al., 2006)	24
Figure 2.13 A diagram of arc-discharge setup (Rastogi et al., 2014)	25
Figure 2.14 Schematic diagram of laser ablation method (Rastogi et al., 2014)	25
Figure 2.15 Schematic diagram of chemical vapor deposition method (Rastogi et al., 2014)	26

Figure 2.16	Growth mechanism of multiwalled carbon nanotubes (a) tip growth model and (b) base growth model (Yan et al., 2009)	31
Figure 2.17	SEM images of (a) CNT-montmorillonite and (b) CNT-zeolite (Kadlečíková et al., 2008)	36
Figure 2.18	Schematic diagram of in situ polymerization (Khan, 2016 #10)	
Figure 2.19	Schematic diagram of intercalation of polymer processing (Sinha Ray and Okamoto, 2003b)	39
Figure 2.20	Schematic diagram of melt intercalation processing (Mihindukulasuriya and Lim, 2014)	40
Figure 2.21	Chemical structure of DGEBA and TGDDM (Mustafa et al., 2014)	41
Figure 3.1	Chemical structure of diglycidyl ether of bisphenol-A (DGEBA)(Patil et al., 2013)	44
Figure 3.2	Chemical structure of trimethylhexamethylene diamine (TMD)	45
Figure 3.3	Chemical structure of muscovite (Li et al., 2011a)	46
Figure 3.4	Chemical structure of Cetyltrimethylammonium bromide (CTAB) (Samakande et al., 2008)	48
Figure 3.5	Schematic of the simplified chemical vapor deposition setup	54
Figure 3.6	Figure 3.6: Schematic of set up equipment for preparation of Mus MWCNT by physically mixed	56
Figure 3.7	Schematic flow of fabrication E/Mus MWCNT	57
Figure 3.8	Schematic illustration and micrograph of the indentation mark on the nanotube composites (Lau et al., 2003)(Lau et al., 2003)	62
Figure 3.9	Experimental set up for thermal conductivity measurement (Othuman Mydin et al., 2018)	64
Figure 4.1	XRD analysis of original Mus and Li-Mus at basal spacing d002 with range (a) $2\theta = 10-70^\circ$ and (b) $2\theta = 2.5-10^\circ$	66
Figure 4.2	Schematic diagram of proposed substitution of Li^+ with K^+	68

Figure 4.3	Schematic diagram of proposed substitution of Li ⁺ with K ⁺	68
Figure 4.4	Schematic diagram of proposed substitution of Li ⁺ with K ⁺	68
Figure 4.5	Basal spacing of CTAB/Li-Mus with increasing of the concentration CTAB to Li-Mus (g/g)	72
Figure 4.6	FTIR analysis of original muscovite, Li-Mus and CTAB/Li-Mus	75
Figure 4.7	(a)-(d) FESEM images with magnification of 5,000x and (e)-(h) EDX analysis of original muscovite, 1st Li-Mus, 3rd Li-Mus and CTAB/Li-Mus	78
Figure 4.8	Schematic diagram of the orientation of surfactant ions on the surface of clays (Cipriano et al., 2005)	79
Figure 4.9	HRTEM images of original muscovite with different magnifications (a) 9,900x and (b) 97,000x	81
Figure 4.10	HRTEM images of Li-Mus at different magnifications (a) 9,900x and (b) 97,000x	82
Figure 4.11	HRTEM images of CTAB/Li-Mus (O-Mus) at different magnifications (a) 9,900x and (b) 97,000x	83
Figure 4.12	HRTEM images on fringes of (a) original Mus, (b) Li-Mus and (c) CTAB/Li-Mus	84
Figure 4.13	FESEM images of (a) original muscovite and (b) pure MWCNT at magnification 30 000 and EDX analysis of (c) original muscovite and (d) pure MWCNT	85
Figure 4.14	FESEM images of Mus MWCNT PM at magnification (a) 5000x and (b) 10 000x and (c) EDX analysis of Mus MWCNT PM	87
Figure 4.15	Schematic diagram of physically mixing Mus MWCNT	88
Figure 4.16	FESEM images of Mus MWCNT HYB at magnification (a) 5 000 and 30 000x and (c) EDX analysis of Mus MWCNT HYB	89
Figure 4.17	Schematic diagram of synthesis Mus MWCNT HYB via CVD	90
Figure 4.18	FESEM images of O-Mus MWCNT HYB with different magnifications (a) 5000x, (b) 30,000x, and (c) EDX analysis of O-Mus MWCNT HYB	91

Figure 4.19	Schematic illustration of O-Mus MWCNT HYB	92
Figure 4.20	HRTEM images of Mus MWCNT PM with magnification (a) 4,000x, (b) 145,000x and (c) 400,000x	93
Figure 4.21:	HRTEM images of Mus MWCNT HYB with different magnifications (a) 9,900x, (b) 63,000x, (c) 145,000x and (d) 450,000x	94
Figure 4.22	HRTEM images of O-Mus MWCNT HYB with different magnifications (a) 9,900x, (b) 63,000x, (c) 145,000x and (d) 450,000x	96
Figure 4.23	Illustration of CNT growth mechanism via tip growth (Kumar and Ando, 2010)	97
Figure 4.24	XRD analysis for (a) Original Muscovite, (b) Pure MWCNT, (c) Mus MWCNT PM, (d) Mus/Ni Catalyst (e) Mus MWCNT HYB, and (e) O-Mus/Ni Catalyst and (f) O-Mus MWCNT HYB	100
Figure 4.25	Raman Spectrum of pure MWCNT, Mus MWCNT PM, Mus MWCNT HYB and O-Mus MWCNT HYB	102
Figure 4.26	FTIR spectrum (a) Muscovite, (b) Mus MWCNT PM and (c) Mus MWCNT HYB, (d) O-Mus MWCNT HYB	104
Figure 4.27	Tensile properties of neat epoxy, E/Mus, E/O-Mus, E/Mus CNT and E/O-Mus CNT with 1 wt%, 3 wt% and 5 wt% filler loading; (a) ultimate tensile strength (b) tensile modulus	109
Figure 4.28	Vickers micro-hardness of neat Epoxy, E/Mus, E/O-Mus, E/Mus MWCNT PM, E/Mus MWCNT HYB, E/O-Mus MWCNT HYB as a function of filler loading	114
Figure 4.29	XRD pattern of E/Mus, E/O-Mus, E/Mus CNT and E/O-Mus CNT at different filler loading; i.e 1, 3 and 5 wt %	118
Figure 4.30	FTIR analysis of neat epoxy, E/Mus 5, E/O-Mus 5, E/Mus CNT 5 and E/O-Mus CNT 5	121
Figure 4.31	FESEM images of fracture surface for neat epoxy with different magnifications; (a) 500x and (b) 10,000x	123
Figure 4.32	FESEM images of epoxy with different magnification (a) 500x and (b) 10,000x	123
Figure 4.33	FESEM images of fracture surface for E/O-Mus 5 with different magnifications; (a) 500x and (b) 10,000x	125

Figure 4.34	FESEM images of fracture surface E/Mus MWCNT PM 5 with different magnification (a) 500x, (b) 10,000x and (c) 30,000x	128
Figure 4.35	FESEM images of fracture surface for E/Mus MWCNT HYB 5 with different magnifications (a) 500x and (b) 10,000x	129
Figure 4.36	FESEM images of fracture surface for E/O-Mus MWCNT HYB 5 with different magnifications (a) 500x and (b) 10,000x	130
Figure 4.37	HRTEM images of E/Mus 5 with different magnifications; (a) 5,000x, (b) 9,900x and (c) 71,000x (continued from the previous page)	132
Figure 4.38	HRTEM images of E/O-Mus 5 with different magnifications; (a) 5,000x, (b) 9,900x and (c) 71,000x	134
Figure 4.39	HRTEM images of E/Mus-CNT PM 5 with different magnifications (a) 9,900x, (b) 15,000x and (c) 38,000x	136
Figure 4.40	HRTEM images of E/Mus MWCNT 5 with different magnifications; (a) 9,900x, (b) 15,000x and (c) 38,000x	138
Figure 4.41	HRTEM images of E/O-Mus MWCNT 5 with different magnifications; (a) 9,900x, (b) 15,000x and (c) 38,000x	140
Figure 4.42	Effect of filler types and filler loading on thermal conductive properties of epoxy nanocomposites	143
Figure 4.43	Schematic of heat flow for: (a) neat epoxy, (b) E/Mus (c) E/OMus, (d) E/Mus MWCNT PM, (e) E/Mus MWCNT HYB and (f) E/O-Mus MWCNT HYB	146

LIST OF ABBREVIATIONS

CEC	Cation exchange
CNT	Carbon nanotube
CTAB	Cetyltrimethylammonium bromide
CVD	Chemical vapor deposition
DGEBA	Diglycidyl ether of bisphenol-A
DDM	4,4'-diamino diphenylmethane
DDS	4,4'-diaminodiphenylsulfone
EDA	Ethylenediamine
EDX	Energy Dispersive X-ray
FESEM	Field emission scanning electron microscopy
FTIR	Fourier transmission infrared
HRTEM	High resolution transmission electron microscopy
ICP	Inductively Couple Plasma
MMT	Montmorillonite
O-MMT	Organo montmorillonite
OTAC	Trimethyloctadecylammonium chloride
PBT	Poly(butylene terephthalate)
PE	Polyethylene
PLSN	Polymer layered silicate nanocomposites
PNCs	Polymer nanocomposites
SEM	Scanning electron microscopy
SWCNT	Single-walled carbon nanotubes
TEM	Transmission electron microscopy
TETA	Trithylenetetramine

TMD	Trimethylhexamethylene diamine
TGDDM	Tetraglycidyl-4,4-diamino-diphenylmethane
XRD	X-Ray diffraction

LIST OF SYMBOLS

M_F	Weight of carbon deposits
M_I	Weight of the catalyst before carbon nanotubes growth
n	An integer
λ	wavelength
d	Spacing between planes in the atomic lattice
θ	Angle
h	Plank's constant
E	Energy
I_D	Intensity of D band
I_G	Intensity of G band
F	Applied load
A	Cross sectional area of the specimen (mm^2)
L_0	Original distance between gage marks
L	Distance between gage marks at any time (mm)

PENYEDIAAN DAN PENCIRIAN NANOKOMPOSIT MUSCOVIT- NANOTIUB KARBON/EPOKSI SILIKAT BERLAPIS

ABSTRAK

Kadar penyebaran dan kelekatan yang kurang berkesan di antara nanotub karbon (CNT) dan matriks polimer merupakan masalah yang kritikal ketika mengintegrasikan CNT dalam nanokomposit polimer. Kajian ini memberi tumpuan kepada kesan teknik fabrikasi yang berbeza termasuk pencampuran fizikal dan pemendapan wap kimia (CVD) pada sifat mekanikal dan kekonduksian termal nanokomposit epoksi. Campuran muskovit nanotub karbon lapisan pelbagai (Mus MWCNT PM) secara fizikal juga telah disediakan melalui kaedah penggilingan bola dengan mencampurkan muskovit dan nanotub karbon lapisan pelbagai selama 24 jam pada 20 rpm untuk mengkaji kesan pemprosesan ke atas sifat mekanikal epoksi/muskovit nanotub karbon lapisan pelbagai. Sintesis pengisi hibrid muskovit nanotub karbon lapisan pelbagai (Mus MWCNT HYB) telah disediakan melalui kaedah pemendapan wap kimia (CVD) yang menggunakan nikel dan muscovit sebagai pemangkin substrat di bawah pengaliran gas metana pada suhu 800°C. Untuk meningkatkan penyebaran Mus MWCNT, muscovit pada awalnya diselaraskan dengan litium nitrat dan diikuti oleh setiltrimetilammonium Bromida (CTAB). Pengubahsuaian muskovit menyebabkan peningkatan jarak antara lapisan serta eksfoliasi lapisan silikat yang lebih baik. Organo-muskovit (O-Mus) kemudiannya disintesis melalui CVD. Mus MWCNT dan O-Mus MWCNT serta Mus MWCNT PM yang telah berjaya disintesis telah dikaji menggunakan mikroskop pengimbas pelepasan medan (FESEM), mikroskop elektron transmisi resolusi tinggi, pembelauan sinar X (XRD), Spektrum Raman dan spektroskopi inframerah transformasi Fourier (FTIR) sebelum dicampurkan dengan

resin epoksi. Didapati bahawa fabrikasi hibrid Mus MWCNT melalui CVD menghasilkan morfologi dan struktur yang lebih baik berbanding dengan Mus MWCNT PM. Epoksi terisi pada Mus MWCNT PM, hybrid Mus MWCNT and hibrid O-Mus MWCNT telah disediakan melalui sistem pempolimeran in situ dan nanokomposit epoksi dan dicirikan menggunakan mikroskop pengimbas elektron (SEM) dan mikroskop transmisi elektron (Ertem *et al.*) untuk menilai dispersi pengisi di antara matriks epoksi. Epoksi terisi hibrid Mus MWCNT menunjukkan ciri-ciri tegangan, kekerasan dan termal yang lebih tinggi berbanding epoksi terisi Mus MWCNT PM. Kecenderungan keberkesanan pengukuhan epoksi terisi hibrid Mus MWCNT adalah disebabkan oleh penyebaran dan ikatan antara muka yang baik dalam matriks epoksi. Kajian ini selanjutnya mengkaji kesan organomuskovit pada sifat-sifat epoksi terisi organo muskovit nanotub karbon lapisan pelbagai (O-Mus MWCNT) seperti yang telah disebutkan. Sifat-sifat tegangan dan kekerasan nanokomposit epoksi terisi O-Mus MWCNT menunjukkan prestasi yang lebih baik berbanding muskovit yang tidak dirawat dengan pembebanan pengisi optimum pada 3 wt%. Ikatan longgar O-Mus MWCNT yang tersebar dalam matriks epoksi menunjukkan penyebaran sekata dan interkasi antara muka yang kuat antara pengisi hybrid dan matriks, yang mempengaruhi peningkatan sifat-sifat mekanik nanokomposit epoksi. Kesimpulannya, pengisian O-Mus MWCNT ke dalam matriks epoksi menunjukkan sifat-sifat mekanikal, kekerasan, kekonduksian termal yang lebih baik berbanding epoksi tulen, dengan itu memenuhi objektif penyelidikan.

PREPARATION AND CHARACTERIZATION OF MUSCOVITE-CARBON NANOTUBES/EPOXY LAYERED SILICATE NANOCOMPOSITES

ABSTRACT

The poor dispersion and low interfacial adhesion between carbon nanotubes (CNT) and polymer matrix are the crucial problem when incorporating of CNT in polymer nanocomposites. This work focuses on the effect of different fabrication techniques including physical mixing and chemical vapour deposition (CVD) on the mechanical and thermal conductivity properties of epoxy nanocomposites. The physically mixed muscovite MWCNT (Mus MWCNT PM) was prepared by employing the muscovite with MWCNT using ball milling for 24h at 20 rpm to examine the effect of processing on the mechanical properties of epoxy/muscovite-multiwalled carbon nanotubes. The synthesis of Mus MWCNT hybrid (Mus MWCNT HYB) filler was prepared via chemical vapour deposition (CVD) loaded nickel catalyst and muscovite as a substrate under methane flow at 800 °C. In order to improve the dispersion of the Mus MWCNT, the muscovite clay particles were initially intercalated with lithium nitrate and followed by cetyltrimethylammonium bromide (CTAB). The modification of muscovite resulted in increased basal spacing as well as better exfoliation of the silicate layers. The organo muscovite (O-Mus) was then synthesized via CVD. The successfully synthesized Mus MWCNT and O-Mus MWCNT as well as Mus MWCNT PM were characterized using Field Emission Scanning Electron Microscopy (FESEM), High Resolution Transmission Electron Microscopy, X-Ray Diffraction (XRD), Raman Spectrum, and Fourier Transform Infrared (FTIR) before incorporated with epoxy resin. It was found that the fabrication of Mus MWCNT hybrid via CVD

produce better morphological and structure compared to Mus MWCNT PM. Mus MWCNT PM, Mus MWCNT HYB and O-Mus MWCNT HYB filled epoxy were prepared by in situ polymerization and the epoxy nanocomposites system and were characterised using scanning electron microscopy (SEM) and transmission electron microscopy to evaluate the dispersibility of filler within the epoxy matrix. The Mus MWCNT HYB filled epoxy showed higher tensile, hardness, and thermal properties compared to Mus MWCNT PM filled epoxy. The high reinforcing efficiency of Mus MWCNT HYB filled epoxy nanocomposites can be attributed to the good dispersion and interfacial interaction within the epoxy matrix. The research explored the effect of organo muscovite on the properties described above of epoxy incorporated organo muscovite multiwalled carbon nanotubes (O-Mus MWCNT). The tensile and hardness properties of the O-Mus MWCNT filled epoxy nanocomposites exhibited better performance as compared to the untreated muscovite with the optimum filler loading at 3 wt%. Further, the loosely entangled O-Mus MWCNT dispersed in epoxy matrix indicated homogeneous dispersion and strong interfacial interaction between the hybrid filler and matrix, which influenced the enhancement of the mechanical properties of the epoxy nanocomposites. Therefore, it is concluded that the incorporation of O-Mus MWCNT into the epoxy matrix exhibited enhanced properties of mechanical, hardness, thermal conductivity compared to the neat epoxy, therefore satisfactorily meeting the objectives of this study.

CHAPTER ONE

INTRODUCTION

1.1 Background

Polymer nanocomposites (PNCs) and their potential application have continued to attract huge interest and attention (Homminga *et al.*, 2005; Moniruzzaman and Winey, 2006; Spitalsky *et al.*, 2010). Compared to pristine polymers or conventional micro and macro-composites, it has been observed during the past decades that the addition of low contents of the nanofillers into the polymer can lead improvement in mechanical, thermal and electrical, flammability resistance, and gas barrier properties (Alexandre and Dubois, 2000). Various types of nanofiller such as nanoclays (Duleba *et al.*, 2014; Souza *et al.*, 2014), graphene (Potts *et al.*, 2011; Song *et al.*, 2012), carbon nanotubes (Broza *et al.*, 2007) and halloysite (Lin *et al.*, 2011) have been incorporated with different polymers to obtain polymer nanocomposites. The evaluation of the nanofiller dispersion is the key ingredient in the polymer matrix in producing polymer nanocomposites with remarkable properties (Bitinis *et al.*, 2011; Esawi and Farag, 2014). Polymer nanocomposites can be prepared by four different methods: in situ polymerization, melt intercalation, solvent mixing and sol-gel techniques (Alexandre and Dubois, 2000).

Nanoclay belongs to a class of materials generally made of layered silicates or clay minerals with traces of metal oxides and organic matter. The most commonly used layered silicate in nanocomposites belongs to the structural family known as the 2:1 phyllosilicates. Montmorillonite and saponite are classified in the 2:1 structure and are among the most commonly used due to their high cation exchange capacity, swelling capacity, strong adsorption and absorption capacities (Becker *et al.*, 2002; Wang and

TABLE OF CONTENTS

	Page
ACKNOWLEDGEMENT	ii
TABLE OF CONTENTS	iii
LIST OF TABLES	viii
LIST OF FIGURES	iv
LIST OF ABBREVIATIONS	xiv
LIST OF SYMBOLS	xvi
ABSTRAK	xv
ABSTRACT	xvii
 CHAPTER ONE: INTRODUCTION	
1.1 Background	1
1.2 Problem Statement	3
1.3 Objectives of the Research	7
1.4 Structure of the Thesis	7
 CHAPTER TWO: LITERATURE REVIEW	
2.1 Polymer Nanocomposites	9
2.2 Layered Silicate	11
2.2.1 Montmorillonite	13
2.2.2 Muscovite	14
2.3 Muscovite Clay Modification	15
2.3.1 Grinding and Delamination	16
2.3.2 Ion Exchange Reaction	17
2.4 Structure and Properties of Modified Layered Silicate	21

2.5	Carbon Nanotubes	22
2.6	Synthesis of Carbon Nanotubes	24
2.6.1	Arc Discharge	24
2.6.2	Laser Ablation	25
2.6.3	Chemical Vapor Deposition	26
2.7	Factors that Affected CNT Growth	26
2.7.1	Catalyst	26
2.7.2	Catalyst Supports	27
2.7.3	Catalyst-Support Interaction	28
2.7.4	Carbon Precursor	29
2.8	Growth mechanism of MWCNT	29
2.9	Carbon Nanotubes Polymer Nanocomposites	31
2.10	Dispersion of Carbon Nanotubes	31
2.10.1	Mechanical Dispersion	32
2.10.2	Chemical Functionalization of Carbon Nanotubes	33
2.10.3	Hybridization of CNTs-Inorganic	34
2.11	Clay-Carbon Nanotubes Hybrid	34
2.12	Preparation of Polymer Nanocomposites	36
2.12.1	In Situ Polymerization	37
2.12.2	Solution Blending	38
2.12.3	Melt Mixing	39
2.13	Epoxy	40
2.14	Epoxy Nanocomposites	41

CHAPTER THREE: EXPERIMENTAL

3.1	Materials	44
3.1.1	Epoxy Resin	44
3.1.2	Hardener	45
3.1.3	Muscovite	45
3.1.4	Lithium Nitrate (LiNO_3)	46
3.1.5	Cetyltrimethylammonium Bromide (CTAB)	47
3.1.6	Nickel (II) Nitrate Hexahydrate	48
3.1.7	Sodium Hydroxide	48
3.1.8	Multiwalled Carbon Nanotubes (MWCNT)	49
3.2	Gases	50
3.2.1	Methane	50
3.2.2	Nitrogen	50
3.2.3	Hydrogen	51
3.3	Clay Modification	52
3.3.1	LiNO_3 Treatment of Muscovite	52
3.3.2	Intercalation of Li-muscovite with CTA^+	52
3.4	Synthesis of Multiwalled Carbon Nanotubes by Chemical Vapor Deposition (CVD)	53
3.4.1	Catalyst Preparation	53
3.4.2	Synthesis of Mus MWCNT Hybrid	54
3.4.3	Preparation of Mus MWCNT by Physical Mixing	55
3.5	Fabrication of Polymer Nanocomposites	56
3.6	Sample Characterization	58
3.6.1	X-ray Diffraction Analysis (XRD)	58
3.6.2	X-ray Fluorescence (XRF)	59

3.6.3	Energy Dispersive X-Ray (EDX)	59
3.6.4	Inductively Couple Plasma- Optical Emission Spectrometer (ICP)	59
3.6.5	CHN Elemental Analysis	60
3.6.6	Fourier Transmission Infrared (FTIR)	60
3.6.7	Raman Spectroscopy	61
3.7	Mechanical Testing	61
3.7.1	Tensile Test	61
3.7.2	Microhardness Test	61
3.8	Morphological Studies	62
3.8.1	Field Emission Scanning Electron Microscopy (FESEM)	62
3.8.2	High Resolution Transmission Electron Microscopy (HRTEM)	63
3.9	Thermal Testing	
3.9.1	Thermal Conductivity Analysis	63
 CHAPTER FOUR: RESULT AND DISCUSSION		
4.1	Effect of Ion Exchange Treatment on Muscovite Clay	65
4.1.1	X-ray Diffraction (XRD)	65
4.1.2	Elemental Analysis	72
4.1.3	Fourier Transform Analysis (FTIR)	74
4.1.4	Field Emission Scanning Eletron Microscopy (FESEM)	76
4.1.5	High Resolution Transmission Electron Microscopy (HRTEM)	79
4.2	Effect of Organo Muscovite on Synthesis Multiwalled Carbon Nanotubes	84
4.2.1	Field Emission Scanning Electron Microscopy (FESEM)	84

4.2.2	High Resolution Transmission Electron Microscopy (HRTEM)	92
4.2.3	X-Ray Diffraction (XRD)	97
4.2.4	Raman Analysis	100
4.2.5	Fourier Transform Infrared (FTIR)	103
4.3	Mechanical Properties of E/Mus MWCNT Nanocomposites	104
4.3.1	Tensile Properties	104
4.3.2	Microhardness properties	112
4.3.3	X-Ray Diffraction (XRD) analysis	116
4.3.4	Fourier Transform Infrared (FTIR) analysis	119
4.3.5	Field Emission Scanning Electron Microscopy	122
4.3.6	High Resolution Transmission Electron Microscopy	131
4.4	Thermal Properties	141
4.4.1	Thermal Conductivity	141
 CHAPTER FIVE: CONCLUSION AND SUGGESTION FOR FUTURE WORKS		
5.1	Conclusion	147
5.2	Suggestion for Future Work	148
 REFERENCES		149

LIST OF TABLES

		Page
Table 3.1	Properties of purchased epoxy resin (Euro Chemo-Pharma MSDS)	44
Table 3.2	Properties of purchased epoxy hardener (Euro Chemo-Pharma MSDS)	45
Table 3.3	Properties of muscovite (Bidor Mineral Sdn. Bhd. MSDS)	46
Table 3.4	Properties of lithium nitrate supplied (Alfa Aesar MSDS)	47
Table 3.5	Properties of supplied CTAB (Merck MSDS)	48
Table 3.6	Chemical and physical properties of nickel (II) nitrate hexahydrate (MerckChemical MSDS)	48
Table 3.7	Details on Sodium Hydroxide (NaOH)	49
Table 3.8	Properties of MWCNT purchased from SkySpring Nanomaterials Inc.	49
Table 3.9	Information of the purchased methane gas.	50
Table 3.10	Information of the purchased nitrogen gas.	51
Table 3.11	Information of the purchased hydrogen gas.	51
Table 3.12	Description of the filler	56
Table 3.13	Description of the composite samples	57
Table 4.1	Main elemental composition of original Mus, Li-Mus, and CTAB/Li-Mus	74
Table 4.2	Raman Intensity of pure MWCNT, Mus MWCNT PM, Mus MWCNT HYB and O-Mus MWCNT HYB	103
Table 4.3	Summarized of tensile properties for different epoxy nanocomposites systems	112
Table 4.4	Average Vickers Hardness of neat epoxy, E/Mus, E/O-Mus, E/Mus MWCNT PM, E/Mus MWCNT HYB, and E/O-Mus MWCNT HYB with different filler loading	155
Table 4.5	Average data of thermal conductivity at different filler loading	144

LIST OF FIGURES

	Page
Figure 2.1 Classification of polymer layered silicate structure (Loganathan, 2017)	11
Figure 2.2 Structures of 2:1 layered silicate (Alexandre and Dubois, 2000)	12
Figure 2.3 Profile model of Na-montmorillonite (Na-MMT) (Paul and Robeson, 2008; Newton et al., 2017)	13
Figure 2.4 Muscovite structure model (de Poel et al., 2014)	15
Figure 2.5 SEM images of muscovite particles after (a) knife mills, (b) ball mill, (c) vibratory mill and (d) sonication process (Santos et al., 2011)	17
Figure 2.6 Intercalation of layered silicate clays into organo clays via ion exchange intercalation (Anastasiadis et al., 2008)	18
Figure 2.7 Molecular model of the intercalation of Cu into muscovite (Friedrich et al., 2007)	19
Figure 2.8 SEM images of (a) original muscovite and (b) muscovite after LiNO ₃ treatment (Yu et al., 2006a)	20
Figure 2.9 (a) SEM images of OTAC intercalated with Li-muscovite and (b) XRD analysis of the intercalated muscovite (Jia et al., 2015)	21
Figure 2.10 Possible arrangements of alkylammonium (Lagaly, 1986)	22
Figure 2.11 Classification of chirality types (Steel, 2015)	23
Figure 2.12 Schematic representation of rolling graphene layer to create CNT (Wu et al., 2006)	24
Figure 2.13 A diagram of arc-discharge setup (Rastogi et al., 2014)	25
Figure 2.14 Schematic diagram of laser ablation method (Rastogi et al., 2014)	25
Figure 2.15 Schematic diagram of chemical vapor deposition method (Rastogi et al., 2014)	26

Figure 2.16	Growth mechanism of multiwalled carbon nanotubes (a) tip growth model and (b) base growth model (Yan et al., 2009)	31
Figure 2.17	SEM images of (a) CNT-montmorillonite and (b) CNT-zeolite (Kadlečíková et al., 2008)	36
Figure 2.18	Schematic diagram of in situ polymerization (Khan, 2016 #10)	
Figure 2.19	Schematic diagram of intercalation of polymer processing (Sinha Ray and Okamoto, 2003b)	39
Figure 2.20	Schematic diagram of melt intercalation processing (Mihindukulasuriya and Lim, 2014)	40
Figure 2.21	Chemical structure of DGEBA and TGDDM (Mustafa et al., 2014)	41
Figure 3.1	Chemical structure of diglycidyl ether of bisphenol-A (DGEBA)(Patil et al., 2013)	44
Figure 3.2	Chemical structure of trimethylhexamethylene diamine (TMD)	45
Figure 3.3	Chemical structure of muscovite (Li et al., 2011a)	46
Figure 3.4	Chemical structure of Cetyltrimethylammonium bromide (CTAB) (Samakande et al., 2008)	48
Figure 3.5	Schematic of the simplified chemical vapor deposition setup	54
Figure 3.6	Figure 3.6: Schematic of set up equipment for preparation of Mus MWCNT by physically mixed	56
Figure 3.7	Schematic flow of fabrication E/Mus MWCNT	57
Figure 3.8	Schematic illustration and micrograph of the indentation mark on the nanotube composites (Lau et al., 2003)(Lau et al., 2003)	62
Figure 3.9	Experimental set up for thermal conductivity measurement (Othuman Mydin et al., 2018)	64
Figure 4.1	XRD analysis of original Mus and Li-Mus at basal spacing d002 with range (a) $2\theta = 10-70^\circ$ and (b) $2\theta = 2.5-10^\circ$	66
Figure 4.2	Schematic diagram of proposed substitution of Li^+ with K^+	68

Figure 4.3	Schematic diagram of proposed substitution of Li ⁺ with K ⁺	68
Figure 4.4	Schematic diagram of proposed substitution of Li ⁺ with K ⁺	68
Figure 4.5	Basal spacing of CTAB/Li-Mus with increasing of the concentration CTAB to Li-Mus (g/g)	72
Figure 4.6	FTIR analysis of original muscovite, Li-Mus and CTAB/Li-Mus	75
Figure 4.7	(a)-(d) FESEM images with magnification of 5,000x and (e)-(h) EDX analysis of original muscovite, 1st Li-Mus, 3rd Li-Mus and CTAB/Li-Mus	78
Figure 4.8	Schematic diagram of the orientation of surfactant ions on the surface of clays (Cipriano et al., 2005)	79
Figure 4.9	HRTEM images of original muscovite with different magnifications (a) 9,900x and (b) 97,000x	81
Figure 4.10	HRTEM images of Li-Mus at different magnifications (a) 9,900x and (b) 97,000x	82
Figure 4.11	HRTEM images of CTAB/Li-Mus (O-Mus) at different magnifications (a) 9,900x and (b) 97,000x	83
Figure 4.12	HRTEM images on fringes of (a) original Mus, (b) Li-Mus and (c) CTAB/Li-Mus	84
Figure 4.13	FESEM images of (a) original muscovite and (b) pure MWCNT at magnification 30 000 and EDX analysis of (c) original muscovite and (d) pure MWCNT	85
Figure 4.14	FESEM images of Mus MWCNT PM at magnification (a) 5000x and (b) 10 000x and (c) EDX analysis of Mus MWCNT PM	87
Figure 4.15	Schematic diagram of physically mixing Mus MWCNT	88
Figure 4.16	FESEM images of Mus MWCNT HYB at magnification (a) 5 000 and 30 000x and (c) EDX analysis of Mus MWCNT HYB	89
Figure 4.17	Schematic diagram of synthesis Mus MWCNT HYB via CVD	90
Figure 4.18	FESEM images of O-Mus MWCNT HYB with different magnifications (a) 5000x, (b) 30,000x, and (c) EDX analysis of O-Mus MWCNT HYB	91

Figure 4.19	Schematic illustration of O-Mus MWCNT HYB	92
Figure 4.20	HRTEM images of Mus MWCNT PM with magnification (a) 4,000x, (b) 145,000x and (c) 400,000x	93
Figure 4.21:	HRTEM images of Mus MWCNT HYB with different magnifications (a) 9,900x, (b) 63,000x, (c) 145,000x and (d) 450,000x	94
Figure 4.22	HRTEM images of O-Mus MWCNT HYB with different magnifications (a) 9,900x, (b) 63,000x, (c) 145,000x and (d) 450,000x	96
Figure 4.23	Illustration of CNT growth mechanism via tip growth (Kumar and Ando, 2010)	97
Figure 4.24	XRD analysis for (a) Original Muscovite, (b) Pure MWCNT, (c) Mus MWCNT PM, (d) Mus/Ni Catalyst (e) Mus MWCNT HYB, and (e) O-Mus/Ni Catalyst and (f) O-Mus MWCNT HYB	100
Figure 4.25	Raman Spectrum of pure MWCNT, Mus MWCNT PM, Mus MWCNT HYB and O-Mus MWCNT HYB	102
Figure 4.26	FTIR spectrum (a) Muscovite, (b) Mus MWCNT PM and (c) Mus MWCNT HYB, (d) O-Mus MWCNT HYB	104
Figure 4.27	Tensile properties of neat epoxy, E/Mus, E/O-Mus, E/Mus CNT and E/O-Mus CNT with 1 wt%, 3 wt% and 5 wt% filler loading; (a) ultimate tensile strength (b) tensile modulus	109
Figure 4.28	Vickers micro-hardness of neat Epoxy, E/Mus, E/O-Mus, E/Mus MWCNT PM, E/Mus MWCNT HYB, E/O-Mus MWCNT HYB as a function of filler loading	114
Figure 4.29	XRD pattern of E/Mus, E/O-Mus, E/Mus CNT and E/O-Mus CNT at different filler loading; i.e 1, 3 and 5 wt %	118
Figure 4.30	FTIR analysis of neat epoxy, E/Mus 5, E/O-Mus 5, E/Mus CNT 5 and E/O-Mus CNT 5	121
Figure 4.31	FESEM images of fracture surface for neat epoxy with different magnifications; (a) 500x and (b) 10,000x	123
Figure 4.32	FESEM images of epoxy with different magnification (a) 500x and (b) 10,000x	123
Figure 4.33	FESEM images of fracture surface for E/O-Mus 5 with different magnifications; (a) 500x and (b) 10,000x	125

Figure 4.34	FESEM images of fracture surface E/Mus MWCNT PM 5 with different magnification (a) 500x, (b) 10,000x and (c) 30,000x	128
Figure 4.35	FESEM images of fracture surface for E/Mus MWCNT HYB 5 with different magnifications (a) 500x and (b) 10,000x	129
Figure 4.36	FESEM images of fracture surface for E/O-Mus MWCNT HYB 5 with different magnifications (a) 500x and (b) 10,000x	130
Figure 4.37	HRTEM images of E/Mus 5 with different magnifications; (a) 5,000x, (b) 9,900x and (c) 71,000x (continued from the previous page)	132
Figure 4.38	HRTEM images of E/O-Mus 5 with different magnifications; (a) 5,000x, (b) 9,900x and (c) 71,000x	134
Figure 4.39	HRTEM images of E/Mus-CNT PM 5 with different magnifications (a) 9,900x, (b) 15,000x and (c) 38,000x	136
Figure 4.40	HRTEM images of E/Mus MWCNT 5 with different magnifications; (a) 9,900x, (b) 15,000x and (c) 38,000x	138
Figure 4.41	HRTEM images of E/O-Mus MWCNT 5 with different magnifications; (a) 9,900x, (b) 15,000x and (c) 38,000x	140
Figure 4.42	Effect of filler types and filler loading on thermal conductive properties of epoxy nanocomposites	143
Figure 4.43	Schematic of heat flow for: (a) neat epoxy, (b) E/Mus (c) E/OMus, (d) E/Mus MWCNT PM, (e) E/Mus MWCNT HYB and (f) E/O-Mus MWCNT HYB	146

LIST OF ABBREVIATIONS

CEC	Cation exchange
CNT	Carbon nanotube
CTAB	Cetyltrimethylammonium bromide
CVD	Chemical vapor deposition
DGEBA	Diglycidyl ether of bisphenol-A
DDM	4,4'-diamino diphenylmethane
DDS	4,4'-diaminodiphenylsulfone
EDA	Ethylenediamine
EDX	Energy Dispersive X-ray
FESEM	Field emission scanning electron microscopy
FTIR	Fourier transmission infrared
HRTEM	High resolution transmission electron microscopy
ICP	Inductively Couple Plasma
MMT	Montmorillonite
O-MMT	Organo montmorillonite
OTAC	Trimethyloctadecylammonium chloride
PBT	Poly(butylene terephthalate)
PE	Polyethylene
PLSN	Polymer layered silicate nanocomposites
PNCs	Polymer nanocomposites
SEM	Scanning electron microscopy
SWCNT	Single-walled carbon nanotubes
TEM	Transmission electron microscopy
TETA	Trithylenetetramine

TMD	Trimethylhexamethylene diamine
TGDDM	Tetraglycidyl-4,4-diamino-diphenylmethane
XRD	X-Ray diffraction

LIST OF SYMBOLS

M_F	Weight of carbon deposits
M_I	Weight of the catalyst before carbon nanotubes growth
n	An integer
λ	wavelength
d	Spacing between planes in the atomic lattice
θ	Angle
h	Plank's constant
E	Energy
I_D	Intensity of D band
I_G	Intensity of G band
F	Applied load
A	Cross sectional area of the specimen (mm^2)
L_0	Original distance between gage marks
L	Distance between gage marks at any time (mm)

PENYEDIAAN DAN PENCIRIAN NANOKOMPOSIT MUSCOVIT- NANOTIUB KARBON/EPOKSI SILIKAT BERLAPIS

ABSTRAK

Kadar penyebaran dan kelekatan yang kurang berkesan di antara nanotub karbon (CNT) dan matriks polimer merupakan masalah yang kritikal ketika mengintegrasikan CNT dalam nanokomposit polimer. Kajian ini memberi tumpuan kepada kesan teknik fabrikasi yang berbeza termasuk pencampuran fizikal dan pemendapan wap kimia (CVD) pada sifat mekanikal dan kekonduksian termal nanokomposit epoksi. Campuran muskovit nanotub karbon lapisan pelbagai (Mus MWCNT PM) secara fizikal juga telah disediakan melalui kaedah penggilingan bola dengan mencampurkan muskovit dan nanotub karbon lapisan pelbagai selama 24 jam pada 20 rpm untuk mengkaji kesan pemprosesan ke atas sifat mekanikal epoksi/muskovit nanotub karbon lapisan pelbagai. Sintesis pengisi hibrid muskovit nanotub karbon lapisan pelbagai (Mus MWCNT HYB) telah disediakan melalui kaedah pemendapan wap kimia (CVD) yang menggunakan nikel dan muscovit sebagai pemangkin substrat di bawah pengaliran gas metana pada suhu 800°C. Untuk meningkatkan penyebaran Mus MWCNT, muscovit pada awalnya diselaraskan dengan litium nitrat dan diikuti oleh setiltrimetilammonium Bromida (CTAB). Pengubahsuaian muskovit menyebabkan peningkatan jarak antara lapisan serta eksfoliasi lapisan silikat yang lebih baik. Organo-muskovit (O-Mus) kemudiannya disintesis melalui CVD. Mus MWCNT dan O-Mus MWCNT serta Mus MWCNT PM yang telah berjaya disintesis telah dikaji menggunakan mikroskop pengimbas pelepasan medan (FESEM), mikroskop elektron transmisi resolusi tinggi, pembelauan sinar X (XRD), Spektrum Raman dan spektroskopi inframerah transformasi Fourier (FTIR) sebelum dicampurkan dengan

resin epoksi. Didapati bahawa fabrikasi hibrid Mus MWCNT melalui CVD menghasilkan morfologi dan struktur yang lebih baik berbanding dengan Mus MWCNT PM. Epoksi terisi pada Mus MWCNT PM, hybrid Mus MWCNT and hibrid O-Mus MWCNT telah disediakan melalui sistem pempolimeran in situ dan nanokomposit epoksi dan dicirikan menggunakan mikroskop pengimbas elektron (SEM) dan mikroskop transmisi elektron (Ertem *et al.*) untuk menilai dispersi pengisi di antara matriks epoksi. Epoksi terisi hibrid Mus MWCNT menunjukkan ciri-ciri tegangan, kekerasan dan termal yang lebih tinggi berbanding epoksi terisi Mus MWCNT PM. Kecenderungan keberkesanan pengukuhan epoksi terisi hibrid Mus MWCNT adalah disebabkan oleh penyebaran dan ikatan antara muka yang baik dalam matriks epoksi. Kajian ini selanjutnya mengkaji kesan organomuskovit pada sifat-sifat epoksi terisi organo muskovit nanotub karbon lapisan pelbagai (O-Mus MWCNT) seperti yang telah disebutkan. Sifat-sifat tegangan dan kekerasan nanokomposit epoksi terisi O-Mus MWCNT menunjukkan prestasi yang lebih baik berbanding muskovit yang tidak dirawat dengan pembebanan pengisi optimum pada 3 wt%. Ikatan longgar O-Mus MWCNT yang tersebar dalam matriks epoksi menunjukkan penyebaran sekata dan interkasi antara muka yang kuat antara pengisi hybrid dan matriks, yang mempengaruhi peningkatan sifat-sifat mekanik nanokomposit epoksi. Kesimpulannya, pengisian O-Mus MWCNT ke dalam matriks epoksi menunjukkan sifat-sifat mekanikal, kekerasan, kekonduksian termal yang lebih baik berbanding epoksi tulen, dengan itu memenuhi objektif penyelidikan.

PREPARATION AND CHARACTERIZATION OF MUSCOVITE-CARBON NANOTUBES/EPOXY LAYERED SILICATE NANOCOMPOSITES

ABSTRACT

The poor dispersion and low interfacial adhesion between carbon nanotubes (CNT) and polymer matrix are the crucial problem when incorporating of CNT in polymer nanocomposites. This work focuses on the effect of different fabrication techniques including physical mixing and chemical vapour deposition (CVD) on the mechanical and thermal conductivity properties of epoxy nanocomposites. The physically mixed muscovite MWCNT (Mus MWCNT PM) was prepared by employing the muscovite with MWCNT using ball milling for 24h at 20 rpm to examine the effect of processing on the mechanical properties of epoxy/muscovite-multiwalled carbon nanotubes. The synthesis of Mus MWCNT hybrid (Mus MWCNT HYB) filler was prepared via chemical vapour deposition (CVD) loaded nickel catalyst and muscovite as a substrate under methane flow at 800 °C. In order to improve the dispersion of the Mus MWCNT, the muscovite clay particles were initially intercalated with lithium nitrate and followed by cetyltrimethylammonium bromide (CTAB). The modification of muscovite resulted in increased basal spacing as well as better exfoliation of the silicate layers. The organo muscovite (O-Mus) was then synthesized via CVD. The successfully synthesized Mus MWCNT and O-Mus MWCNT as well as Mus MWCNT PM were characterized using Field Emission Scanning Electron Microscopy (FESEM), High Resolution Transmission Electron Microscopy, X-Ray Diffraction (XRD), Raman Spectrum, and Fourier Transform Infrared (FTIR) before incorporated with epoxy resin. It was found that the fabrication of Mus MWCNT hybrid via CVD

produce better morphological and structure compared to Mus MWCNT PM. Mus MWCNT PM, Mus MWCNT HYB and O-Mus MWCNT HYB filled epoxy were prepared by in situ polymerization and the epoxy nanocomposites system and were characterised using scanning electron microscopy (SEM) and transmission electron microscopy to evaluate the dispersibility of filler within the epoxy matrix. The Mus MWCNT HYB filled epoxy showed higher tensile, hardness, and thermal properties compared to Mus MWCNT PM filled epoxy. The high reinforcing efficiency of Mus MWCNT HYB filled epoxy nanocomposites can be attributed to the good dispersion and interfacial interaction within the epoxy matrix. The research explored the effect of organo muscovite on the properties described above of epoxy incorporated organo muscovite multiwalled carbon nanotubes (O-Mus MWCNT). The tensile and hardness properties of the O-Mus MWCNT filled epoxy nanocomposites exhibited better performance as compared to the untreated muscovite with the optimum filler loading at 3 wt%. Further, the loosely entangled O-Mus MWCNT dispersed in epoxy matrix indicated homogeneous dispersion and strong interfacial interaction between the hybrid filler and matrix, which influenced the enhancement of the mechanical properties of the epoxy nanocomposites. Therefore, it is concluded that the incorporation of O-Mus MWCNT into the epoxy matrix exhibited enhanced properties of mechanical, hardness, thermal conductivity compared to the neat epoxy, therefore satisfactorily meeting the objectives of this study.

Wang, 2008). Another silicate layer with a similar nature, Muscovite ($\text{KAl}_2(\text{AlSi}_3\text{O}_{10})(\text{OH})_2$), has become a more promising reinforcement than other conventional layered silicate with particular interest due to its smooth, well-defined surface of the muscovite sheet, excellent corona resistance and insulation properties (Pashley and Quirk, 1989). The use of layered silicate as a reinforcement is hindered due to two major problems: (i) the layered silicate is not easily dispersed in polymers due to their preferred face stacking in agglomerates tactoids and (ii) the tactoids cannot be dispersed into discrete monolayer due to the intrinsic incompatibility of hydrophilic layered silicate with hydrophobic polymer (Pavlidou and Papaspyrides, 2008). Long-chain alkylammonium surfactants were usually employed to modify the silicate interlayer galleries by ion exchange treatment in order to weaken the interaction between adjacent layers and to enhance the compatibility of the silicate layer with the polymer matrix (Yu *et al.*, 2004). The replacement of inorganic exchange cations with organic ions on the surface of silicate layers is useful to expand the silicate layered galleries.

Compare to different range of nanofillers, carbon nanotubes (CNT) have emerged as the most potential candidate nanofiller for polymeric materials composites due to their remarkable high strength and stiffness and exhibit an exceptionally high aspect ratio (Coleman *et al.*, 2006). The carbon nanotubes can be classified into either multiwalled (MWCNT) or single walled (SWCNT) depending on the preparation method. There are three commonly-used method of CNT synthesis; arc discharge, laser vaporation and chemical vapor deposition (CVD) (Kumar and Ando, 2010). A number of studies on carbon based polymer nanocomposites have been carried out taking different polymer matrix including polyethylene (PE) (Morcom *et al.*, 2010), polypropylene (Al-Saleh, 2015), polyamide (So *et al.*, 2007), and polyurethane

(Ryszkowska *et al.*, 2007).

Incorporating the hybrid nanofillers with two geometrically dissimilar nanomaterials; 1D multiwalled carbon nanotubes (MWCNT) and 2D silicate layer as reinforcing fillers is more interesting in the polymer matrix owing to its significant synergetic effects (Milone *et al.*, 2010; Mitchell *et al.*, 2002). Several studies on the synthesis of carbon nanotubes supported on layered silicate (clay) hybrid filler via chemical vapour deposition have previously been reported (Li *et al.*, 2009; Manikandan *et al.*, 2012a; Wang *et al.*, 2006b). In fact, it has been shown that the dispersion of small amounts of carbon nanotubes (CNT) or clay in the polymer matrix will lead to excellent mechanical, thermal and electrical properties of the final composites (Montazeri *et al.*, 2010; Wang *et al.*, 2010). The previous researcher used clay as catalytic support for carbon nanotubes (CNTs) growth in order to form a unique 3D nanostructured hybrid filler to fabricate polymer nanocomposites (Gournis *et al.*, 2002).

1.2 Problem Statement

Epoxy is one of the most common thermosetting polymers that widely used in industrial applications due to their excellent mechanical and chemical properties, such as high tensile and compression strength and good chemical resistance to solvent (Chen *et al.*, 2007). Epoxy-based nanocomposites are known to have superior properties over neat epoxy which is brittle and shows poor crack propagation resistance (Liu *et al.*, 2005). There are a few approaches to extend the properties of epoxy resin by using micro-size filler materials modifying the brittle epoxy to improve toughness and rigidity (Sandler *et al.*, 2003). The addition of filler generally leads to

an increase in Young's modulus and a reduction in the ultimate elongation of the matrix. Despite, the toughening efficiency of the micro-sized particles is much lower as a result of the rigid particles cannot effectively stop crack propagation (Lee and Yee, 2000). Another develops system offering promising results to reinforce epoxy matrix with nano-sized organic and inorganic filler such as carbon nanotubes (CNT), nanoclays and carbon nanofibers (Al-Saleh and Sundararaj, 2009; Kim *et al.*, 2008; Polizos *et al.*, 2011; Puglia *et al.*, 2003; Sinha Ray and Okamoto, 2003b; Wang *et al.*, 2006a; Zappalorto *et al.*, 2015). This approach has attracted considerable interest because of the notable increase in the mechanical and thermal properties of epoxy nanocomposites with the addition of small amounts of nanoparticles (Iara Ferreira *et al.*, 2012). In fact, the mechanical properties are largely governed by the interfacial interaction between filler and polymers. (Wong *et al.*, 2003) studied the adhesion between CNT and polymer in nanocomposites and suggested that in some cases CNT are covalently bonded to the polymer matrix. It was reported that the interfacial bonding strength can be improve by adding trace amount of other materials such as graphene between the carbon nanotubes and polymer matrix (Li *et al.*, 2011b).

Generally, the main factors in producing remarkable polymer carbon nanotubes nanocomposites are the homogeneous dispersion of the individual MWCNT into the polymer matrix and good interfacial interaction between MWCNTs and polymer matrix (Ma *et al.*, 2010). Unfavourably, MWCNT tend to agglomerate due to their high aspect ratio and van der Waals interactions, leading to many defect sites limiting the efficiency of MWCNT on polymer matrix (Breuer and Sundararaj, 2004; Rastogi *et al.*, 2008). With concern of the above issues, several modification methods were introduced to improve the dispersion of CNT in polymer matrix. Previous approaches for improving dispersion CNT with mechanical dispersion (i.e.

ball milling and sonication) by adjusting the nanotubes length are commonly employed. Despite of the effectiveness of mechanical dispersion techniques to shorten the CNT, the process, could in fact, damage the carbon nanotube (CNT) structure (Kukovecz *et al.*, 2005; Tucho *et al.*, 2010). In another approaches, functionalization of CNT appears to be a particular interest to improve the quality of the filler-matrix interface by introducing covalent linkages between the CNT and the functional group (Cha *et al.*, 2016; Davari *et al.*, 2014). Acid functionalization of MWCNT with $\text{H}_2\text{SO}_4/\text{HNO}_3$ has shown significant property enhancement in Young Modulus, tensile strength and fracture strain in CNT/epoxy polysulfide nanocomposites (Shirkavand Hadavand *et al.*, 2013). Unfortunately, the yields of the functionalised CNT decreased, and the CNT structure was damaged due to the highly corrosive strong acids (HNO_3 and H_2SO_4) used (Tsai *et al.*, 2013). Further to the above, CNT hybridization using inorganic filler has gain attention of researchers because it has shown capacity to improve CNT dispersion without damage the structure. Chemical vapor deposition (CVD) is commonly approach for the production of CNT. This method has been use for a broad range of inorganic substrate such as silica (Qian *et al.*, 2010), alumina (Nagaraju *et al.*, 2002; Zakaria *et al.*, 2014) and clay (Manikandan *et al.*, 2013; Pastorková *et al.*, 2012). A different study on the synthesis of clay-carbon nanotube (CNT) hybrids has recently been carried out, recognizing that clay minerals; montmorillonite (Madaleno *et al.*, 2012b; Manikandan *et al.*, 2013), zeolite (Kadlečíková *et al.*, 2008) ,kaolinite, and bentonite (Allaadini *et al.*, 2016). (Manikandan *et al.*, 2013) reported on the successfully synthesis of carbon nanotubes on montmorillonite supported iron catalyst by chemical vapor deposition (CVD). The CNT obtained were uniform, smooth and straight with nanotubes diameter less than 15 nm. Nevertheless, limited literature has been published regarding the growth of

carbon nanotubes on muscovite particles via CVD (Kudus *et al.*, 2012).

It is well established that the clay mineral are ideal support materials for developing support metal catalyst (Cheng, 1999; Zhang *et al.*, 2006). Montmorillonite (MMT) are categorized into 2:1 structures are among the most commonly clay used as support materials for the synthesis of carbon nanotubes (Madaleno *et al.*, 2012b; Manikandan *et al.*, 2013) as well as a reinforcement filler in fabricating polymer layered silicate nanocomposites (Gârea *et al.*, 2008; Ilyin *et al.*, 2015). The growing of polymer layered silicate nanocomposites evolved from a conventional clay (MMT) to an alternative clay (muscovite) due to their interesting structural features including; high aspect ratio, high flexibility, high toughness, and electrical insulating properties (Daji *et al.*, 2015; Jia *et al.*, 2017; Liaw *et al.*, 2011). Particularly, muscovite are not readily dispersed in polymer matrix due to their face-to-face stacking in agglomerates tactoids (Pavlidou and Papaspyrides, 2008). Moreover, in contrast to the other expandable clay minerals such as vermiculite and MMT, muscovite neither swells nor can be delaminated under ambient conditions (Gaines, 1957; Osman and Suter, 1999) due to the very high layer charge density and homogeneous distribution resulting from the outside tetrahedral sheet of the aluminosilicate layer (Yu *et al.*, 2006a). Based on this concern, specific surface modification of muscovite was carried out in order to fully utilize outstanding performance of muscovite. The muscovite was modified with two steps ion exchange treatment in order to further enlarge the basal spacing of muscovite particles which includes; (i) lithium nitrate intercalation and (ii) CTAB intercalation (Yu, 2007). According to Fornes *et al.* (2002), the larger interlayer spacing may lead to easier exfoliation which could facilitate the insertion of polymer chains. Hsu *et al.* (2009) has reported, the increasing distance between clay layers

facilitates to easier diffusion of NiO particles onto the surface of clay platelets.

1.3 Objectives of the Research

In the present work, the muscovite MWCNT hybrid compound were prepared and analyzed in order to fabricate in epoxy nanocomposites. The main goals in this study:

- 1) To investigate the effect of fabrication technique of muscovite MWCNT filler on the morphological structure, mechanical, hardness and thermal properties of the epoxy nanocomposites
- 2) To study the effect of modification of organo muscovite within epoxy nanocomposites on morphological, mechanical and thermal properties.

1.4 Structure of the Thesis

The thesis is organized into five chapters.

Chapter One: Presents the scope of the study including a general overview, problem statement, main objectives and structure of the thesis.

Chapter Two: Describes the basic concepts of polymer-layered silicate nanocomposites including the structure of polymer-layered silicate nanocomposites, method of preparation, clay modification, structural and properties of modified clay, including a case study on polymer-layered silicate nanocomposites. This chapter also provides details on the synthesis of carbon nanotubes; growth mechanism, properties, and clay/carbon nanotubes hybrid filler.

Chapter Three: Provides a detailed description of the materials and the experimental design on the synthesis of Mus MWCNT via chemical vapour deposition (CVD) and physically mix, surface modification of muscovite clay, fabrication of epoxy incorporated muscovite, O-Mus, Mus MWCNT and O-Mus MWCNT

nanocomposites. The preparation and testing of all epoxy systems are discussed in subsequent sections.

Chapter Four:

4.1 Describes the process involved in the surface modification on muscovite clay to improve the interfacial interaction of the clay with MWCNT and epoxy matrix. This chapter further describes the two steps of intercalation used to modify the Muscovite clay; (1) replacing K^+ in the interlayer of muscovite by melting $LiNO_3$ and (2) intercalation of alkylammonium surfactants into $LiNO_3$ -muscovite using hydrothermal reactor.

4.2 Discuss the preparation of Mus MWCNT HYB, O-Mus MWCNT HYB via CVD synthesis and Mus MWCNT PM by ball milling. The final composites compound was characterized by Field Emission Scanning Electron Microscopy (FESEM), High Resolution Transmission Electron Microscopy (HRTEM), X-Ray Diffraction (XRD), Fourier Transmission Infrared (FTIR) and Raman Spectroscopy.

4.3 Describe the achievement and good dispersion of Mus MWCNT within the epoxy matrix via in situ polymerization. The effects of different filler are investigated on the morphological, mechanical and thermal conductivity of the O-Mus MWCNT/epoxy nanocomposites.

Chapter Five: Provides the overall conclusion of the study based on the work performed, summarising the key findings of the epoxy nanocomposites for all types of nanofiller. Lastly, limitations of the study and suggestions for future research are presented.

CHAPTER TWO

LITERATURE REVIEW

2.1 Polymer Nanocomposites

Polymer nanocomposites (PNCs) may be defined as a hybrid of two or more materials, where the matrix is a polymer and the dispersed phase at least one dimensional smaller than 100 nm (Muller *et al.*, 2017). Over the last decades, it has been observed that the addition of low content of the nanofillers into polymer matrix can improved their mechanical, thermal, barrier and flammability properties (Bitinis *et al.*, 2011; Muller *et al.*, 2017). Nanofiller can be categorized on their basis of their dimensions; one dimensional which includes nanotubes and nanowires, two dimensional such as nanoclay (Okada and Usuki, 2006) and graphene (Fasolino *et al.*, 2007) and three dimensional such as spherical (Liu *et al.*, 1997) and cubical nanoparticles (Huang *et al.*, 2003). Among all the available nanofiller for polymer composites, those derived from layered silicates (clay) and carbon nanotubes (CNT) are the most studied (Al-Saleh, 2015; Arash *et al.*, 2014; Lakshmi *et al.*, 2008; Souza *et al.*, 2014). There are two concerns that are extremely important of the polymer nanocomposites with full potential of properties enhancement; (i) homogeneous dispersion of the filler in the polymer matrix and (ii) strong interfacial interaction between filler and polymer matrix . Previous research widely studied the processing and characterization of nanoclay incorporated with different polymeric matrix. (Gopakumar *et al.*, 2002) reported on the improvement of Young modulus by produced exfoliation clay within the polyethylene matrix. (Liu *et al.*, 2005) claimed that the improvement of the organoclay-modified high performance epoxy nanocomposites on toughness and modulus properties by prepared the nanocomposites with direct mixing

method. As well as layered silicate, there are various polymer has been reported to be used to incorporated carbon nanotubes (Al-Saleh, 2015; H. Gojny *et al.*, 2006). (Wu *et al.*, 2015; Zhou *et al.*, 2008b) reported on the improvement on flexural, glass transition temperature and decomposing temperature of CNT-epoxy nanocomposites prepared by ultrasonic cavitation method.

The microstructure of the polymer layered silicate nanocomposites generated depending on the interfacial interaction between the polymer matrix and layered silicate (modified or unmodified). Polymer layered silicate nanocomposites can be classified as intercalated, exfoliated, and phase separated composites as depicted in Figure 2.1:

- (a) Intercalated nanocomposites: obtained when polymer chains intercalated between the silicate layers, leading to a well-ordered multilayer structure with a repeat distance between them.
- (b) Exfoliated nanocomposites: obtained when the clay layers are well separated from one another and individually dispersed in the continuous polymer matrix.
- (c) Phase separated: poor interaction between the polymer matrix and clay layers results in relatively poor mechanical performance.

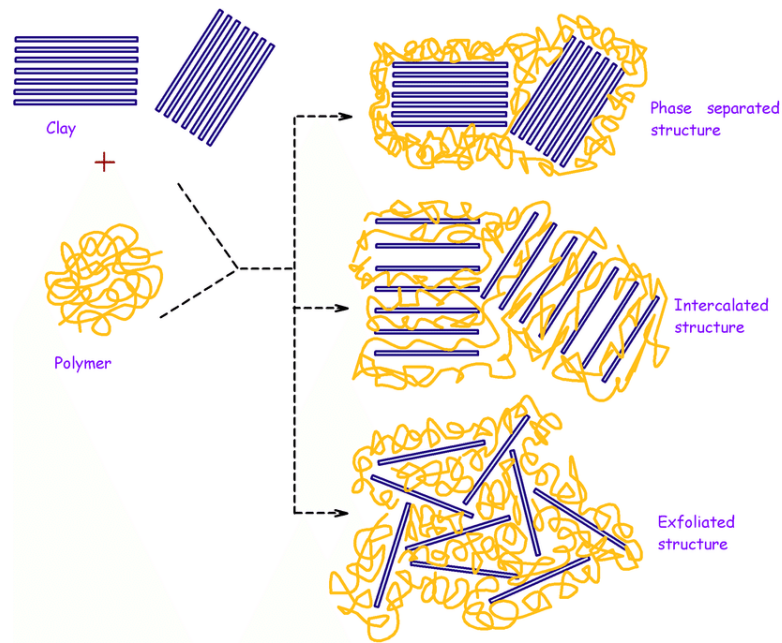


Figure 2.1: Classification of polymer layered silicate structure (Loganathan, 2017)

2.2 Layered Silicate

Layered silicates are clay minerals, built of two structural units. Layered silicate can be divided into three major groups:

- In 1:1 layered structure (kaolinite) a tetrahedral sheet is fused with octahedral sheet, whereby the oxygen atoms are shared.
- For 2:1 layered silicates (2:1 phyllosilicates, e.g. MMT, vermiculite, and illite), consist of two-dimensional layers where a central octahedral sheet of alumina is fused to two external silicate tetrahedral by the tip, which is the oxygen ions of the octahedral sheet also belong to the tetrahedral sheets.
- Meanwhile, 2:2 type layered silicate (chlorite) composed of four crystal sheets, which the crystal sheets of silica tetrahedron and alumina or magnesium octahedron is alternately arranged (Ke and Stroeve, 2005).

The layered structure that commonly used in the preparation of polymer layered silicate nanocomposites are from the smectite family with 2:1 structure. MMT, hectorite and saponite have been most investigated due to their swelling behaviour and ion exchange properties. Their crystal lattice consists of two silica tetrahedral sheet fused to an edge-shared octahedral sheet typically aluminum or magnesium hydroxide as shown in Figure 2.2. Periodic stacking of the layers forms a lattice, with each layer of approximately 1nm thickness and the lateral dimensions vary from 300 Å to several microns depending on the particular silicate. Stacking of the layers with a regular van der Waals gap in between are called the interlayer or the gallery (Alexandre and Dubois, 2000; Kiliaris and Papaspyrides, 2010). The net charge deficiency is typically compensated by cations, such as Na^+ , K^+ and Ca^{2+} in the interlayer gallery.

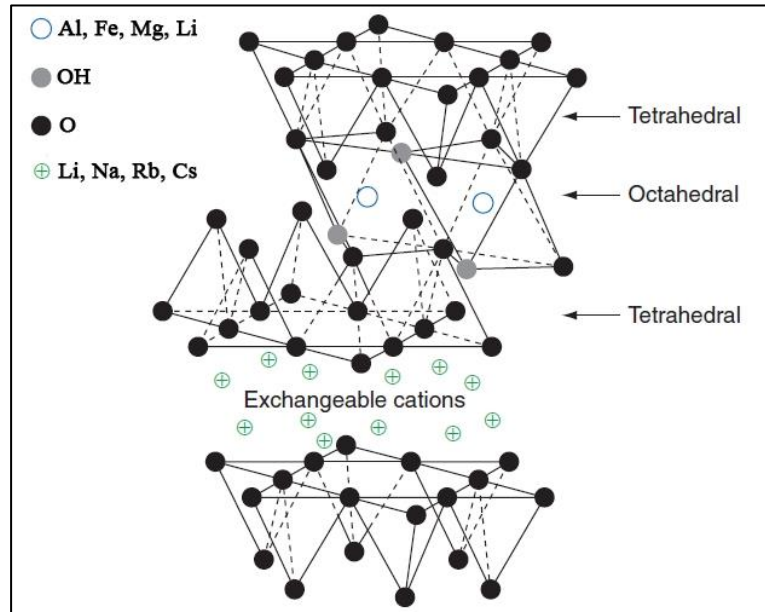


Figure 2.2: Structures of 2:1 layered silicate (Alexandre and Dubois, 2000)

2.2.1 Montmorillonite

Montmorillonite is a clay mineral with a sandwich structure composed of two tetrahedral sheets and a central alumina octahedral sheet. All positions at the top and base of the lattice layers of MMT are completely occupied by oxygen atom, which the layers are held together by weak van der Waal's forces. Figure 2.3 shows the model structure of Na-MMT. Thus, water molecule easily penetrate the interlayer region and expand the lattice interlayer. In addition, the clay layer was negatively charge due to the substitution of Mg^{2+} or Fe^{2+} for Al^{3+} in octahedral sheets and substitution of Al^{3+} for Si^{4+} in tetrahedral sheets, which is counterbalanced by exchangeable cations in the galleries between layers (Tjong, 2006). In their pristine form, their excess negative is balanced by cations (Na^+ , Li^+ , Ca^+). The interlayer cations can be replaced easily either by organic or inorganic molecules through an intercalation (Pramanik *et al.*, 2001). Previous studies have demonstrated that the surfactant cations with long-chain alkylammonium cations intercalated into the interlayer through an exchange reaction formed a great enhancement of the MMT properties (Widjonarko *et al.*, 2018).

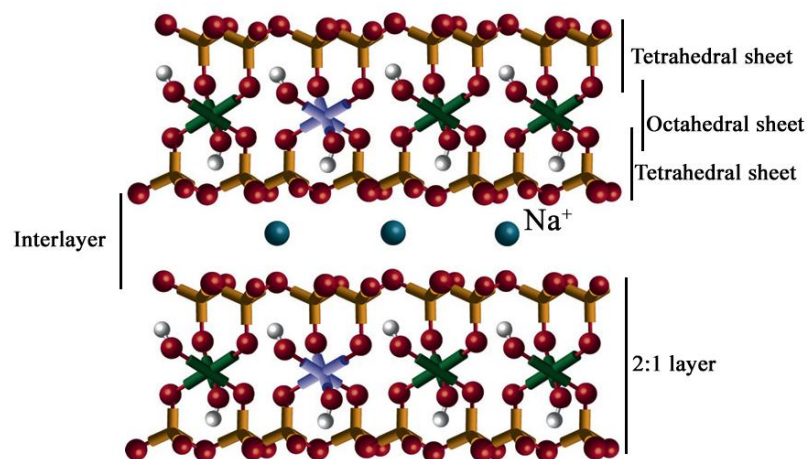


Figure 2.3 : Profile model of Na-montmorillonite (Na-MMT) (Newton *et al.*, 2017; Paul and Robeson, 2008)

2.2.2 Muscovite

Muscovite with ideal composition of $\text{KAl}_2(\text{AlSi}_3\text{O}_{10})(\text{OH})_2$ is a 2:1 phyllosilicate mineral has become an attractive reinforcement in polymer layered silicate nanocomposites due to its well-defined structure, outstanding corona resistance, high aspect ratio (larger than MMT), and its available in large amounts at a relatively low cost (Kornmann *et al.*, 2002). Muscovite belongs to monoclinic structure with the space group (C2/c), with the cell parameter $a = 5.18 \text{ \AA}$, $b = 8.99 \text{ \AA}$, $c = 20.07 \text{ \AA}$, $\beta = 95.751^\circ$ (Liang and Hawthorne, 1996). The crystal structure comprises of Al-O-Al octahedral (O) layers sandwiches between two Si-O-Al tetrahedral (T) layers. The crystal structure of muscovite model is shown in Figure 2.4. In tetrahedral layers, silicon atoms randomly occupy (75%) of the tetrahedral sites, and aluminum atoms occupy the remaining sites. Meanwhile, in dioctahedral layers, 2/3 octahedral sites are occupy by aluminum atoms, and the rest are vacant (McKeown David *et al.*, 1999). Substitution of lattice Si^{4+} by Al^{3+} in tetrahedral layer and Fe^{2+} or Mg^{2+} and Ca^{2+} for Al^{3+} in the octahedral layer resulting in a net negative charge on the basal surfaces and alkali ion, mainly K^+ , is attracted in the interlayer to counterbalance the charge of layers (Tamura *et al.*, 2008). The interlayer cations such as K^+ or Na^+ strengthen the bonding between basal planes of T-O-T sheets which are normally held by attractive van der Waals forces, through the attractive electrostatic interactions (Schlegel *et al.*, 2006). Due to charge deficiency of the layers and the presence of interlayer cations, there is strong columbic interaction between the adjacent layers besides the van der Waals, which are normally monotonically attractive and occur between all molecules (A. Osman and Suter, 2000; Osman *et al.*, 1999). These forces, consequently, render muscovite particles non swelling in aqueous environment. The presence of the aluminol groups ($-\text{AlOH}$) exposed at its edge surface acquires muscovite hydrophilic

character and hence, primarily limits its dispersion in an organic matrix (e.g. polymer).

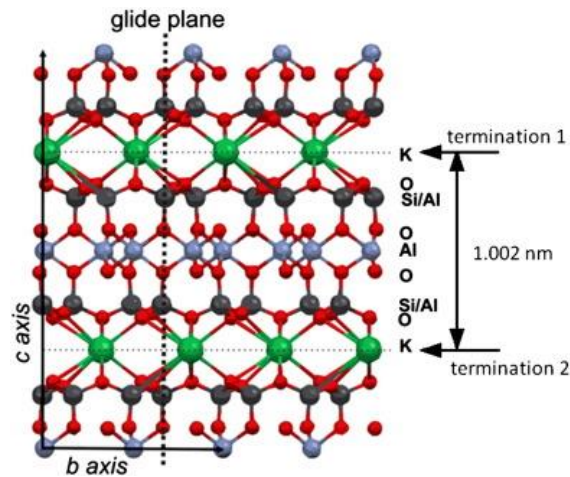


Figure 2.4: Muscovite structure model (de Poel *et al.*, 2014)

2.3 Muscovite Clay Modification

Modification of the muscovite will increase the interlayer spacing thus, polymers, nanometer metallic oxide and metal ions could intercalate into muscovite galleries to form specialized nanocomposites. There are two major issues that should be considered in order to utilize the outstanding of performance of muscovite in polymer layered silicate nanocomposites; (a) muscovite are difficult to dispersed due to face to face stacking in agglomerates tactoids and (b) muscovite tactoids are difficult to disperse into discrete monolayers due to their intrinsic incompatibility of hydrophilic layered silicate with hydrophobic polymers (Pavlidou and Papaspyrides, 2008). However, compared to other 2:1 layered silicate, the interlayer cations of muscovite are difficult to access and are not exchangeable under normal conditions (Osman *et al.*, 1999; Osman and Suter, 1999). Specific modifications were carried out to improve the quality and characteristics of the muscovite such as; grinding, delamination and intercalation (ion exchange).

2.3.1 Grinding and Delamination

Grinding is a common method in modification of clay that resulting in; particle size reduction (delamination and lateral size reduction), produce rearrangement of the coordination of clay and diffusion within the structure of atoms (mainly protons) (Jr. Reynolds and Bish, 2002; Madrid Sanchez Del Villar and Sánchez-Soto, 1988; Yariv and Lapides, 2000). Grinding (either in dry state, in the presence of water and chemical additives) is commonly used to reduce the muscovite particle size (Papirer *et al.*, 1990). Dry grinding includes ball mill, bar mill and vibratory mills. It is well known that grinding of clay minerals affect the clay structure and characteristics (Sánchez-Soto *et al.*, 2004). However, due to the friction forces and impact during the grinding process, can destroy the platelets of the muscovite while reducing the particle size. Meanwhile, grinding using a knife mill is cheaper (does not use water or liquids) and easier compare to conventional method. Generally, knife mill used to grind high plasticity materials. Figure 2.5 shows muscovite structure after different types of grinding.

On the other hand, delamination describes a process where intercalation occurs; guest material introduces between the layers while the stacking layers is remains. Delamination of muscovite using sonication (wet grinding method) shows decreasing of muscovite thickness (Fontes Santos *et al.*, 2011). Pérez-Cabero *et al.* (2004) demonstrate that the crystalline nanometre and submicron size plate-like mica particles have been prepare from natural macroscopic mica after sonication treatment.

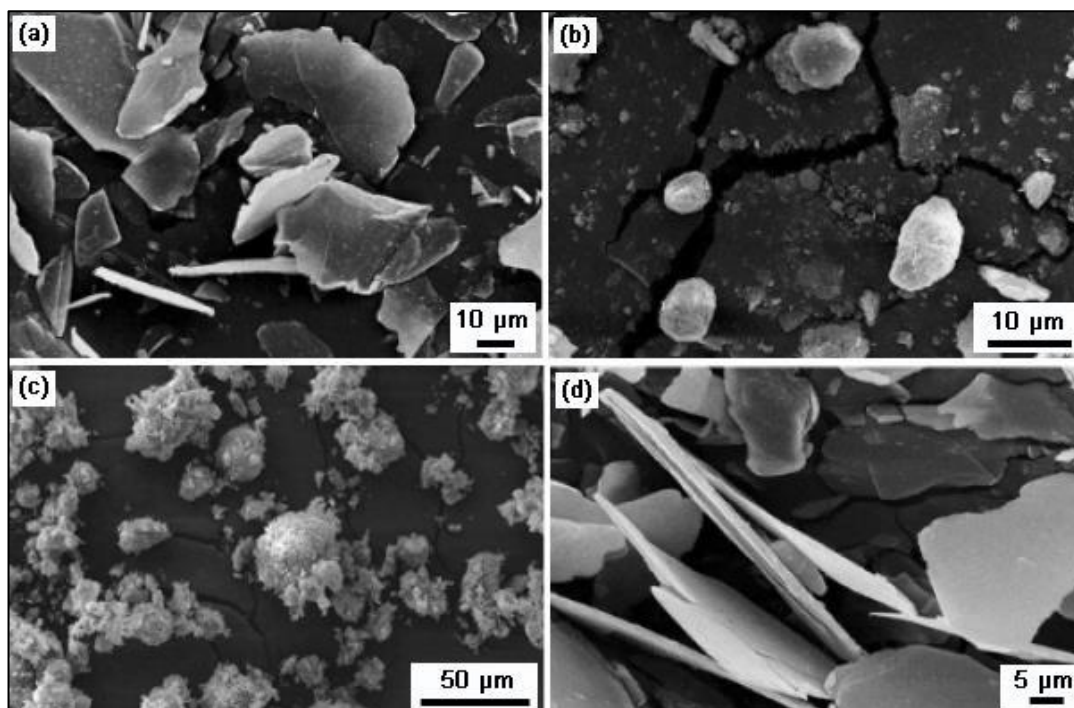


Figure 2.5: SEM images of muscovite particles after (a) knife mills, (b) ball mill, (c) vibratory mill and (d) sonication process (Santos *et al.*, 2011)

2.3.2 Ion Exchange Reaction

The intercalation of organic species into the interlayer region of clay mineral with preservation of the layered structure has been study extensively due to the interesting properties of the modified clay as nanoscale reinforcement filler for polymer materials (Giannelis, 1996). Ion exchange is one of the most common methods for layered silicate modification. This intercalation, which courses with the exchange of the compensating cations of the clay by the organic cations (alkylammonium ion), can improve the interfacial adhesion properties between the clay filler and polymer matrix by transforms the surface of the clay particles from hydrophilic (organophobic) to organophilic (hydrophobic). In addition, the basal spacing of the clays is increased depending on their arrangement in the interlayer region. Figure 2.6 shows the schematic of ion intercalation process. The modification of pristine silicate is carried out by replacing small inorganic cations with any positively charge species of the clay.

The organic modification thus, expands the clay galleries and matches the clay surface polarity with the polarity of polymer (Anastasiadis *et al.*, 2008).

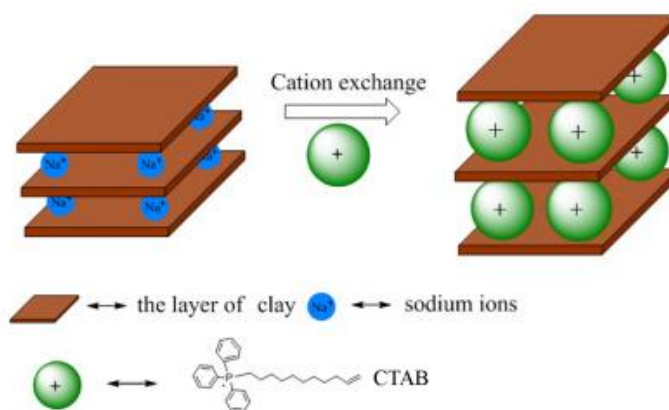


Figure 2.6: Intercalation of layered silicate clays into organo clays via ion exchange intercalation (Anastasiadis *et al.*, 2008)

Most researchers believe that the loss of interlayer K^+ by chemical or mechanical methods may expand the muscovite silicate layers. The replacement of interlayer K in muscovite by other cations has been carried out by previous researcher in order to expand the mineral lattice (Osman and Suter, 1999; Scott and Reed, 1964; Yu *et al.*, 2006a). Scott and Reed (1964) was the early conducted the experiment to remove the interlayer K^+ ions using sodium tetraphenylborate (NaTPB) and sodium chloride (NaCl) resulting in K-depleted. This treatment was reported increased the basal spacing of muscovite from 10 to 12.3Å.

Friedrich *et al.* (2007) has suggest that the intercalation of muscovite with Cu (II), which resulted strong changes in the XRD patterns especially in the range between 3° and 10°. The new broad peak was appeared at $2\theta=3.9^\circ$ and 7.9° while the original peak at d_{002} decreased. The d values of the new peaks show the increase of the interlayer spacing which confirmed that the metal ions are introduced into the interlayer of the muscovite. Meanwhile, the d_{002} of original muscovite are not

disappeared indicates that not all layers are intercalated with Cu metal. Molecular model of Cu intercalation into muscovite was depicted in Figure 2.7.

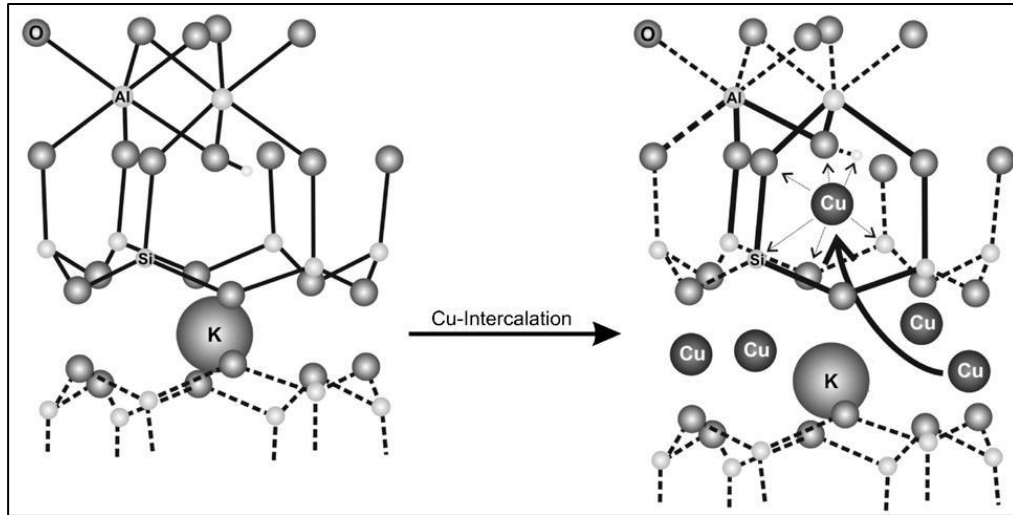


Figure 2.7: Molecular model of the intercalation of Cu into muscovite (Friedrich *et al.*, 2007)

Treating muscovite with molten LiNO_3 at high temperature was frequently employed to prepare delaminated muscovite particles. Yu *et al.* (2006a) reported that the intercalation of muscovite with lithium nitrate increases the d spacing of the silicate layer. The ion exchange of the muscovite was performed by replace the interlayer cations in muscovite with Li^+ by melting lithium nitrate. According to the Scherrer equation, the Li-muscovite had the basal spacing of 24.16\AA , compared with that 19.92\AA of the original muscovite. It indicates that the exchange between Li^+ and K^+ open the interlayers and increase the basal spacing of muscovite providing the possibility of organic cations intercalation (Jia *et al.*, 2015). The Li^+ entered the lattice of muscovite which reduce the layer charge, leading to interlamellar expansion as shown in SEM images in Figure 2.8 (L. White, 1956)

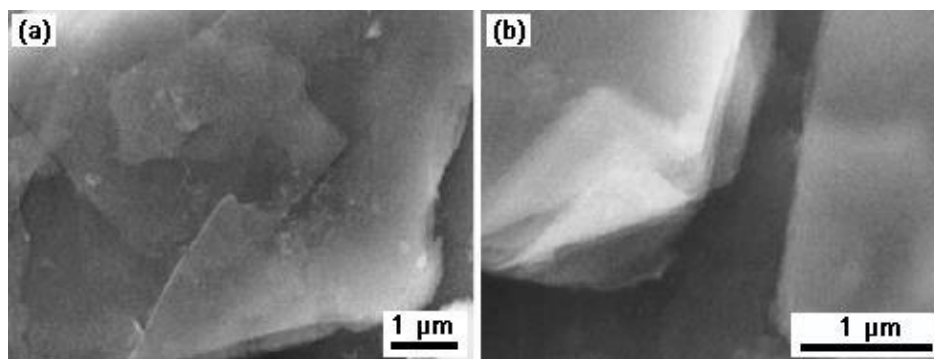


Figure 2.8: SEM images of (a) original muscovite and (b) muscovite after LiNO₃ treatment (Yu *et al.*, 2006a)

The Li-muscovite was further study by using as a host for the intercalation with alkylammonium under hydrothermal reaction. Yu *et al.* (2006b) showed that the diffraction peaks of hydrothermal reaction of Li-muscovite with cetyltrimethylammonium bromide (CTAB) solution at different temperatures moved toward low 2θ compared to Li-muscovite. Furthermore, Yu (2007) study the effect of CTAB concentration on the Li-muscovite structure. It is showed that the arrangement of the CTA⁺ chains depends on the CTAB concentration. At low CTAB concentration, the intercalated CTA⁺ cations with Li-muscovite showed lateral monolayer arrangement. Meanwhile, at highest concentration, the CTA⁺-muscovite showed paraffin-like arrangement with d spacing at 002 diffraction peaks is 27.4Å. In the other study, the distance between Li-muscovite and trimethyloctadecylammonium chloride (OTAC) greatly increased the basal spacing of muscovite to 2.92nm. The SEM images and XRD analysis in Figure 2.9 show the intercalation of OTAC with Li-Mus (Jia *et al.*, 2015).

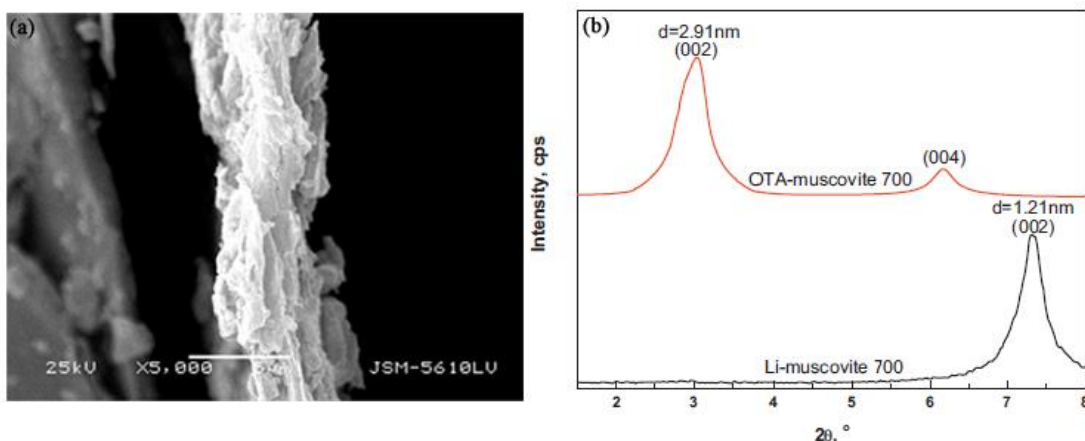


Figure 2.9: (a) SEM images of OTAC intercalated with Li-muscovite and (b) XRD analysis of the intercalated muscovite (Jia *et al.*, 2015)

2.4 Structure and Properties of Modified Layered Silicate

Pristine layered silicates are usually contained hydrated Na^+ and K^+ ions (Heller-Kallai, 1981). Since the pristine state layered silicates are only miscible with hydrophilic polymers such as poly(ethylene oxide) and poly(vinyl alcohol) (Greenland, 1963), in order to render them miscible with other polymers, the hydrophilic silicate surface need to be convert to an organophilic one, by ion exchange reactions with cationic surfactants including primary, secondary, tertiary and quarternaryalkylammonium. Alkylammonium ions are mostly used compared to other onium salts such as sulfonium and phosphonium (Zanetti *et al.*, 2000). The organic cations improve wetting with the polymer matrix (Kornmann *et al.*, 2002). Moreover, as the long organic chains of such surfactants, with positively charged ends, are tethered to the negatively charged silicate layer, resulting in a larger interlayer spacing (Kim *et al.*, 2001). Thus, it is possible for the polymer to diffuse between the layers and eventually separated them (Kornmann *et al.*, 2001; Zerda and J. Lesser, 2011). In addition, both of the cations provide the functional group which can improve the adhesion between inorganic and the polymer matrix (Krishnamoorti *et al.*, 1996).

Figure 2.10 shows example of modified clay structure. Initially, the orientation of surfactant chains was determined using X-ray diffraction (XRD). Depending on the packing density, temperature and alkyl chain length, the chains were thought to lie either parallel to the silicate layers forming mono or bilayers or radiate away from silicate layers forming mono or bimolecular arrangements Polymer-layered silicate nanocomposites: an Overview Peter C. LeBaron, Zhen Wang, Thomas J. Pinnavaia

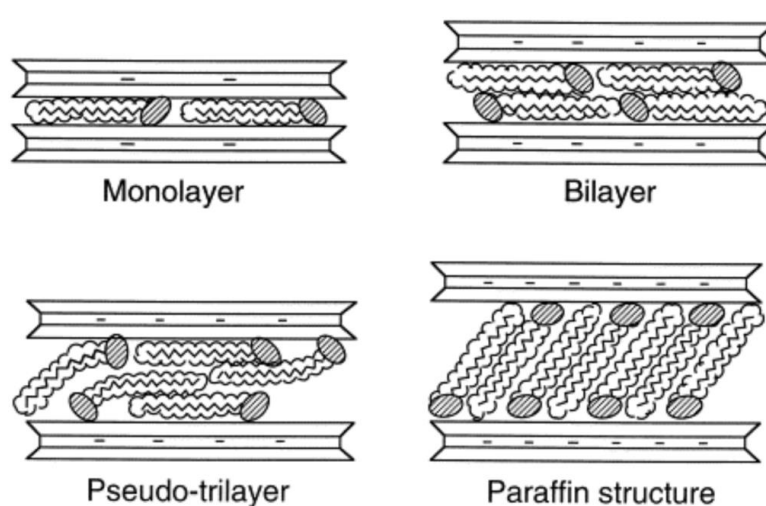


Figure 2.10: Possible arrangements of alkylammonium (Lagaly, 1986)

2.5 Carbon Nanotubes

Since their discovery by Iijima (1991), carbon nanotubes (CNT) have been a major focus of research work to exploit their exceptional properties. CNTs are fullerene-related nanostructures and can be described as a hexagonal network of carbon atoms (graphite sheets) that has been rolled into a hollow cylinder. Basically, there are two types of CNTs; single walled carbon nanotubes (SWCNT) (Bethune *et al.*, 1993; Iijima and Ichihashi, 1993) and multiwalled carbon nanotubes (MWCNT). A single walled carbon nanotube can be considered as a single graphene sheet rolled up into seamless cylinder with typical diameter 1.2-1.4nm. Multiwalled carbon

nanotubes consist of stacking concentric cylinders of several graphene layers with an interlayer separated by 0.4nm. The layers of tube walls are held together by van der Waals forces between adjacent layers, where each layer can have different chirality. According to the rolling angle of the graphene sheet, three types of chirality can be classified into armchair, zigzag and chiral as shown in Figure 2.11 (Dai and Mau, 2001; Steel, 2015)

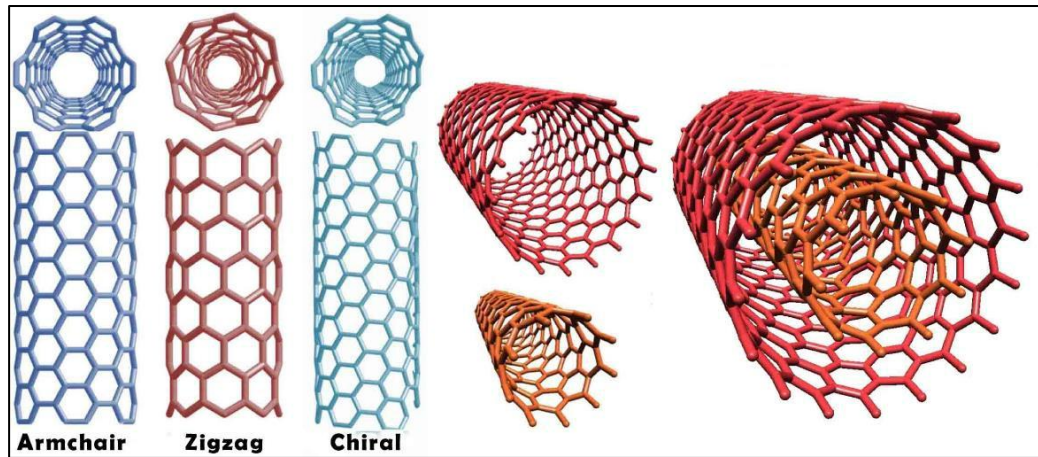


Figure 2.11 : Classification of chirality types (Steel, 2015)

The tube chirality is defined by the chiral vector, $\mathbf{Ch} = n\mathbf{a}_1 + m\mathbf{a}_2$, where the integers (n, m) are the number of steps along the unit vectors (\mathbf{a}_1 and \mathbf{a}_2) of the hexagonal lattice as shown in Figure 2.12 (Wu *et al.*, 2006). The chemical bonding of CNTs are composed entirely of sp^2 bonds and consist of honeycomb lattice with seamless structure, similar to graphite, which provides the molecule with the unique strength (Zhang *et al.*, 2009).

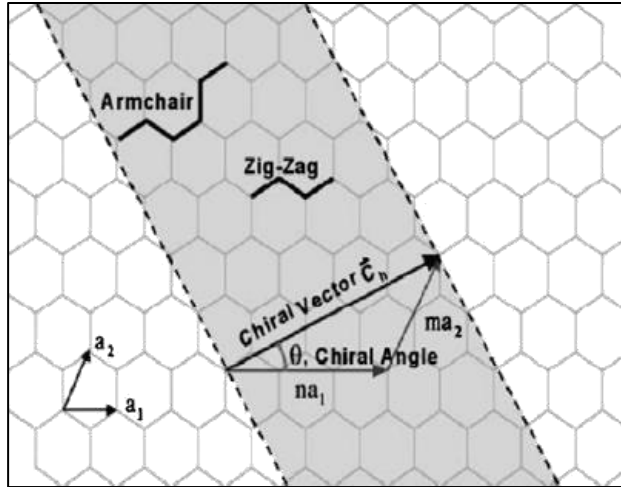


Figure 2.12: Schematic representation of rolling graphene layer to create CNT (Wu *et al.*, 2006)

2.6 Synthesis of Carbon Nanotubes

2.6.1 Arc Discharge

Arc discharge was first use by Iijima (1991) to synthesis CNTs. The tubes were produce using a similar method for the fullerenes synthesis in the past. This technique assembly generated between anode and cathode of carbon electrodes installed in the center of the chamber under an inert gas (i.e. helium). The advantage of this method is easily to be synthesis and can produces in large quantity (Ebbesen and Ajayan, 1992; Journet *et al.*, 1997). However, carbon impurities and encapsulated nanoparticles are usually produced with the CNTs. The schematic of arc discharge setup was shown in Figure 2.13.